Geophys. J. Int. (2006) **164,** 246–258 doi: 10.1111/j.1365-246X.2005.02826.x

Ultrasonic properties of sedimentary rocks: effect of pressure, saturation, frequency and microcracks

Sibylle. I. Mayr and Hans Burkhardt

Department of Applied Geosciences, Technical University Berlin, Ackerstrasse 71 – 76, D – 13355 *Berlin, Germany. E-mail: s.mayr@tu-berlin.de*

Accepted 2005 October 4. Received 2005 September 2; in original form 2004 December 20

ABSTRACT

Seismic velocities and attenuations are influenced by lithology, porosity and permeability as well as the kind and quantity of the pore fluids. The microstructure of rocks is another important factor influencing seismic properties. This influence can be used to investigate the pressure-dependent closure of microcracks. For this purpose, velocities and attenuations of *P* and *S* waves have been determined at ultrasonic frequencies in three different rocks (vacuum dry and partially saturated with water) as a function of hydrostatic pressure up to 200 MPa. A new combined model has been developed. With this model an explicit description of the microstructure [local fluid flow (LF)] and macrostructure (Gassmann effect, global fluid flow) is possible. Assuming a patchy saturation (i.e. inhomogeneous distribution of the fluid in the pores) and modulus reduction, both the saturation-dependent measurements and the pressure-dependent data can be explained. The modelling and the phenomenological interpretation of the data gained under increasing hydrostatic pressure yields consistent results concerning the amount of crack closure as well as the range in which crack closure appears: in high-porosity sandstones (Bentheimer and Obernkirchner Sandstone) a strong closure of cracks already with a small increase of pressure must be concluded. In a low-porosity Harzer Greywacke a significantly lower closure of cracks can be concluded within the pressure range of 0–100 MPa. It is shown, however, that there must be open cracks in all rocks even under elevated hydrostatic pressure, resulting in a measurable effect due to LF.

Key words: attenuation, elastic wave theory, fluids in rocks, laboratory measurements, moduli, sediments.

1 INTRODUCTION

For the lithological interpretation of seismic measurements laboratory measurements are of fundamental interest (e.g. Bourbié *et al.* 1987; Burkhardt *et al.* 1990; Vernik 1996). In the laboratory, rocks can be exposed to various defined conditions. In this way the processes and mechanisms that are effective with elastic wave propagation can be examined under simulated *in situ* conditions. Therefore, pressure dependence of seismic properties has to be measured and understood. For practical reasons most laboratory measurements are conducted in the ultrasonic frequency range (Toksöz & Johnston 1981). For the transfer of the results at ultrasonic frequencies to acoustic and seismic frequencies, it is essential to know the frequency-dependent mechanisms of the elastic wave propagation.

In order to get more information about the rocks in both the laboratory and in the field, attenuation is determined next to the velocities of the compressional and shear waves (e.g. Koesoemadinata & McMechan 2001).

The seismic velocities and attenuation are affected by mineral content, the kind and quantity of the pore fluid, as well as by macroscopically determined quantities like porosity, permeability, bulk and shear modulus of the investigated rocks (Schön 1983, 1997; Bourbié *et al.* 1987; Mörig 1993). Investigations by e.g. Knight & Nolen-Hoeksema (1990), Burkhardt *et al.* (1990, 1992), Murphy (1982), Wulff & Burkhardt (1996, 1997) show the additional influence of the microstructure (i.e. distribution, density, dimension, geometry of the cracks and the constitution of the grain contacts) on seismic attributes.

1.1 Pressure dependence

Previous measurements on sandstones have shown a strong nonlinear increase in seismic velocities with small increase in the hydrostatic pressure. This is observed in dry and in fluid saturated rocks. Concurrently a decrease of the attenuation is also observed. Above a certain pressure—typical for each rock—further increase of velocities with increasing pressure is comparatively small. Different studies (King 1966; Toksöz *et al.* 1979; Freund 1992; King *et al.* 2000) proceed from the assumption, that above this pressure all microcracks in the rocks are closed and the behaviour of the seismic waves should only be influenced by the macroscopic properties and not by the microstructure (e.g. grain contacts, microcracks). Other

studies (Winkler 1985, 1986; Murphy *et al.* 1986; Mavko & Jizba 1991; Mavko & Noelen-Hoeksema 1994; Tao *et al.* 1995; Wulff & Burkhardt 1997) assume the closure of microcracks too, however, they state that even under higher hydrostatic pressure there must be open microcracks in the rock, because the experimental data can only be explained by processes on the microscopic scale [local fluid flow (LF)].

All effects influencing elastic wave propagation at low pressure are effective at high pressure, only their amount is changing: the influence of macrostructure [global fluid flow (GF)] is approximately constant with increasing pressure, whereas the influence of LF decreases significantly due to closure of microcracks. To infer whether there are still open microcracks above a certain pressure both effective fluid flow mechanisms have to be considered, when modelling the pressure dependence of ultrasonic properties: although a contribution will come from LF as long as there are open microcracks, a complete closure of all cracks would imply that only GF would be effective. Therefore, the knowledge of the influence of all mechanisms affecting seismic waves is essential for a thorough understanding of the pressure dependence of the measured velocities and attenuations.

1.2 Elastic wave propagation in saturated rocks

By saturating vacuum dry rocks with polar fluids—for instance water—a reduction of the elastic moduli is observed at all frequency ranges. This *modulus reduction* is a surface effect on grain contacts due to the reduction of surface energy (Johnson *et al.* 1971; Mörig 1993). The amount of the modulus reduction is dependent on the kind of rock and frequency range, and differs between *P* and *S* waves (e.g. Murphy 1982; Burkhardt *et al.* 1986, 1990; King *et al.* 2000).

The *Gassmann effect* (Gassmann 1951) leads to a higher *P*-wave velocity at full saturation, because the pores are filled with a fluid having a high compression modulus compared to gas. The *S* wave is not influenced, because the shear modulus of water and gas are equal to zero. Due to this effect compressional and shear waves in fully and partially saturated rocks are influenced in a different manner (e.g. Mavko & Noelen-Hoeksema 1994).

Knight & Nolen-Hoeksema (1990), Knight *et al.* (1998) and Cadoret *et al.* (1995, 1998) have shown, that the saturation of rocks can either be homogeneous, described by a gas–fluid mixture in the pores, or inhomogeneous, also called patchy saturation, described by a gas-pocket (GP) model. Experiments with different degrees of saturation (Wulff & Burkhardt 1997) have shown that measurements cannot be explained by a homogeneous gas–fluid mixture in the pores but by an inhomogeneous saturation (gas pockets).

A strong frequency dependence of the seismic parameters is observed in saturated rocks, with both polar and non-polar fluids. This is due to GF in the macropores as well as a LF in the micropores (e.g. Murphy 1984; Burkhardt *et al.* 1986, 1990, 1992; Mörig 1993; Knight *et al.* 1998). Both fluid flow mechanisms are band limited relaxation phenomena. In both cases at frequencies well below or above the relaxation frequency f_F the system is in a relaxed or unrelaxed state, respectively, with no attenuation. In the vicinity of the relaxation frequency f_{LF}—the transition between the two states—attenuation increases due to deformation induced viscous fluid flow. The velocities change from lower values (relaxed state) to higher values (unrelaxed state).

The *global fluid flow*—theory (Biot 1956; Biot & Willis 1957) is describing a coupled motion of fluid and matrix, therefore, next to viscosity η and density of fluid ρ_f, the hydraulic permeability κ and porosity ϕ is included in the relaxation frequency:

$$f_{GF} = \frac{\eta}{\rho_f}\frac{\phi}{2\pi\kappa}. \tag{1}$$

The Gassmann effect is included in the theory of Biot.

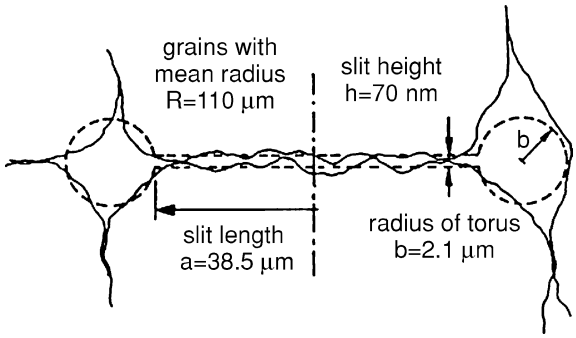

Figure 1. Local fluid flow: geometry of model after Schütt (1992) and Murphy *et al.* (1986). The parameters *R*, *a*, *b* and *h* are valid for Obernkirchner Sandstone.

On the other hand the *local fluid flow* (also called: squirt fluid flow) is influenced by the microstructure. For the description of the LF, different approaches are used, *cf.* Vernik (1996), Wulff & Burkhardt (1996, 1997) and Mavko *et al.* (1998). Some authors (Berryman 1988; Mavko & Jizba 1991; Mavko & Noelen-Hoeksema 1994; Dvorkin & Nur 1993; Parra 1997) have described the effect phenomenologically. Murphy *et al.* (1986) take into account the microstructure explicitly by means of an approximative geometry. In this model, the single grain contact in a sandstone is considered as a parallel combination of an elastic and a viscous element. The elastic element is described by the elastic properties in dry rock. For description of the viscous element, the grain contact is approximated by means of a torus connected by a small disk-like slit. The torus corresponds to bigger pores in the rock, the slit to microcracks (Fig. 1). The fluid in the slit leads to the frequency-dependent LF, which corresponds to the viscous element, that is, the relaxation process. The relaxation frequency f_{LF} depends on the properties of the fluid (bulk modulus K_f and viscosity η) as well as on the grain contact's geometry (aspect ratio = ratio of the microcrack's height *h* to length *a*):

$$f_{LF} = \frac{K_f}{\eta}\left(\frac{h}{a}\right)^n \tag{2}$$

(Murphy *et al.* 1986). The exponent *n* has been found to be 2.4 by varying the aspect ratio h/a in calculating f_{LF} (Mayr 2002). Murphy *et al.* (1986) introduce the crack density γ because the effect of the LF on velocities and attenuations depends on the number of cracks in a rock. Thus the model is able to describe for instance crack closure with increasing pressure. Using Gassmann's relation (Gassmann 1951), the Gassmann effect is included in this LF model.

1.3 Existing combined models

Investigations by, for example, Burkhardt *et al.* (1986, 1990), Mavko & Jizba (1991), Mörig (1993), Mavko & Noelen-Hoeksema (1994), Wulff (1995) and Wulff & Burkhardt (1997) have shown that the propagation of seismic waves in high-porosity rocks is influenced by both GF and LF.

Therefore, combined models and assumptions of Mavko & Jizba (1991), Mavko & Noelen-Hoeksema (1994), Dvorkin & Nur (1993), Wulff (1995), Parra (1997) and Diallo *et al.* (2003) take both fluid

flow mechanisms into account. Some of these models describe only the change in the *P* waves by the squirt flow (Dvorkin & Nur 1993), while others include the LF phenomenologically in the high-frequency approximation (Mavko & Noelen-Hoeksema 1994). None of the existing models includes the microstructure explicitly.

1.4 Strategy

Measurements on various rocks under different saturation conditions at low uniaxial stress in ultrasonic range by Schütt (1992) and Wulff (1995) as well as in the seismic frequency range by Mörig (1993) have been investigated in order to understand the mechanisms effective in saturated sedimentary rocks. The interpretation of these measurements led to theoretical models for description of the measured seismic parameters (e.g. Burkhardt *et al.* 1990, 1992; Schütt 1992; Mörig 1993; Wulff 1995 as well as Wulff & Burkhardt 1996, 1997).

Based on these investigations a new combined model (Biot–Gassmann–Murphy model), which contains the LF and the GF including the Gassmann effect and modulus reduction, was developed to describe the seismic velocities as a function of microscopic and macroscopic parameters (Mayr 2002, and section 3). The LF in this model depends on the microstructure in the same manner as introduced by Murphy *et al.* (1986).

Numerous measurements under defined conditions were used. Firstly, measurements under different saturation conditions at low uniaxial stress (approx. 30 MPa) in the ultrasonic range by Schütt (1992) were reinterpreted to determine and validate the parameters of the newly developed combined model (*cf.* Mayr 2002 and section 3.5). Secondly, three rocks with different properties were chosen to investigate the changing influence of the microstructure under elevated pressure taking into consideration both, *P* and *S* waves. Thus new measurements under hydrostatic pressure (up to 200 MPa) were performed on these rocks and interpreted with the new developed combined model (Mayr 2002). Measurements on vacuum dry rocks reveal the properties of the matrix (Section 4), while measurements on partially saturated rocks yield information on the influence of fluid flow and by this on the pressure induced changes of microstructure of the rocks (Section 5).

2 MEASUREMENTS: METHODS AND SAMPLES USED

2.1 Experimental methods

Attenuation and velocities of *P* and *S* waves at ultrasonic frequencies (0.4–1 Mhz) were determined with an aluminium measurement cell using a buffer technique for measurements in pulse transmission. The attenuation $1/Q$ (with $Q =$ quality factor) was determined with the spectral ratio method (Toksöz *et al.* 1979; and e.g. Wulff & Burkhardt 1997).

For measurements under increasing hydrostatic pressure (Mayr 2002) the samples were protected against the pressure fluid in the vessel with a 3-mm-thick neopren sleeve. Although they were not drained, it can be assumed that the pore pressure is negligible due to the partial saturation (31–73 per cent). Therefore, under these conditions the effective pressure in the rock equals the applied external confining pressure P_c (*cf.* Wulff & Burkhardt 1997). At each pressure three measurements were done directly after reaching this pressure and another three 10 min later. Tests have shown that after 10 min the system (rock and fluid) is stationary. The measured data shown are the average of all measurements at one pressure. Additionally velocity and attenuation were determined at low uniaxial stress (approx. 3.5 MPa) before each hydrostatic pressure cycle as an approximation to zero pressure conditions. The errors in velocity and attenuation determined at hydrostatic pressure are 0.5 per cent for *P*-wave velocities, 1 per cent for *S* waves and 20 per cent for $1/Q_p$ and 30 per cent for $1/Q_s$, respectively (Mayr 2002).

For reinterpretation data from Schütt (1992) are used. He measured v_p and v_s in dependence of water saturation on Obernkirchner Sandstone under uniaxial pressure of 30 MPa.

2.2 Sample description

All samples have a diameter of 80 mm and a height of approximately 30 mm. The sample surfaces were made parallel and polished dry. Measurements under different saturation conditions and the measurements at hydrostatic pressure were done on adjacent samples.

For all measurements on vacuum dry samples, they were stored for at least 4 days at 70°C in a vacuum oven and saturated with dry nitrogen. The partial saturation with distilled water was obtained by drying fully saturated samples controlled by weighting. After reaching the required saturation, the samples were left several days wrapped in aluminium foil to achieve a homogeneous saturation within the sample.

For the experiments under hydrostatic pressure three rocks were chosen: two sandstones (Bentheimer and Obernkirchner Sandstone) with high porosity and microcracks next to larger pores, and a Harzer Greywacke with low porosity due to predominantly microcracks. In Figs 2, 3 and 4 thin sections of the rocks are shown. All these rocks have been investigated by Burkhardt *et al.* (1986, 1990), Schütt (1992), Mörig (1993), Lebedev *et al.* (1996), Schopper & Riepe (1986) and Wulff & Burkhardt (1996, 1997) with respect to mineral and petrophysical qualities and to seismic and ultrasonic properties. They differ significantly in their macroscopic parameters, porosity and permeability, and in the microscopic pore size distribution (Fig. 5). All rocks can be classified as rather homogeneous. The sandstones have a high content of quartz and a very low content of clay (Table 1). Next to quartz the Harzer Greywacke contains feldspar and a small amount of mica and no clay. Petrophysical parameters are listed in Table 2.

3 NEW COMBINED MODEL: GLOBAL AND LOCAL FLUID FLOW

3.1 Concept of the model

Local fluid flow in partially and fully saturated sandstones changes the properties of the rock depending on frequency. This means that the moduli describing the behaviour of the saturated rock are

Table 1. Mineralogical composition (in mass per cent) of Obernkirchner Sandstone (OK) after Lebedev *et al.* (1996) and Harzer Greywacke (HZ) after R. Bussert (private communication) as well as approximate mineralogical composition of Bentheimer Sandstone (BH) after H. Holl (private communication).

Mineral	OK	HZ	BH
Quarz	90.56	59	90-96
Kaolinite	4.99	—	2–4
Muscovite	2.38	2	x
Sphene	1.42	—	x
Albite	0.55	27	x
Chlorite	0.11	3	x
Mikrolin	—	9	x
Cherts			2

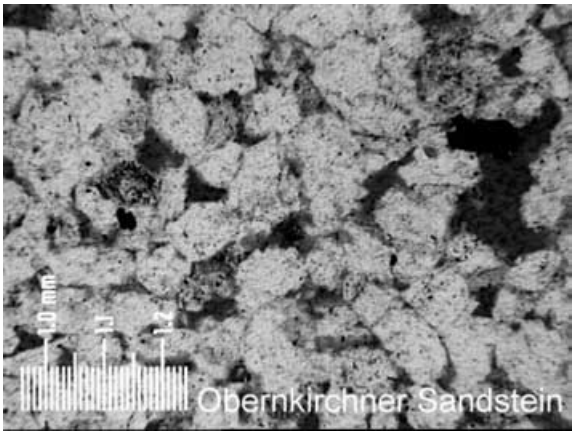

Figure 2. Thin section of Obernkirchner Sandstone (OK): high-porous fine-grained sandstone, Lower Cretaceous, Wealden, quarry Obernkirchen. The pore space is filled with blue harz (dark areas).

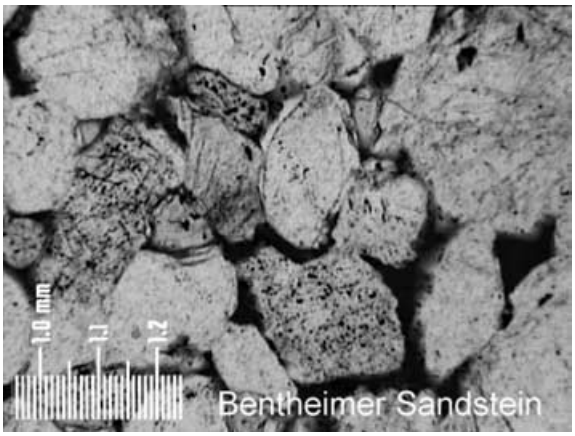

Figure 3. Thin section of Bentheimer Sandstone (BH): Lower Cretaceous, Valendis, quarry Gildehaus; higher porosity than Obernkirchner Sandstone.

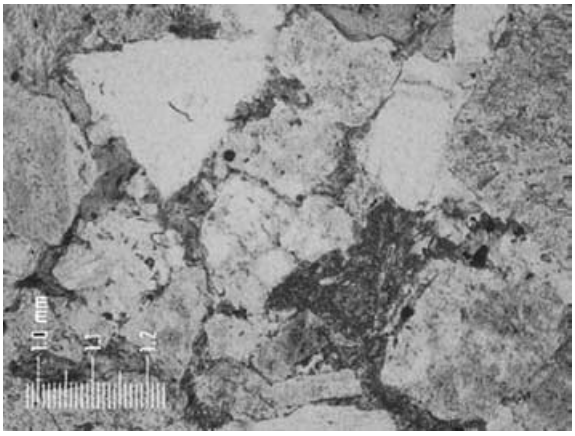

Figure 4. Thin section of Harzer Greywacke (HZ). Lower Carboniferous, outcrop Soesetalsperre. Lower porosity than Obernkirchner Sandstone.

changed by the LF. Thus the real valued elastic bulk and shear moduli (K_b and N) in the basic equations of Biot (1956) are replaced by the frequency-dependent complex-valued moduli (K_{LF} and N_{LF}) of the LF model by Murphy *et al.* (1986). The resulting equations

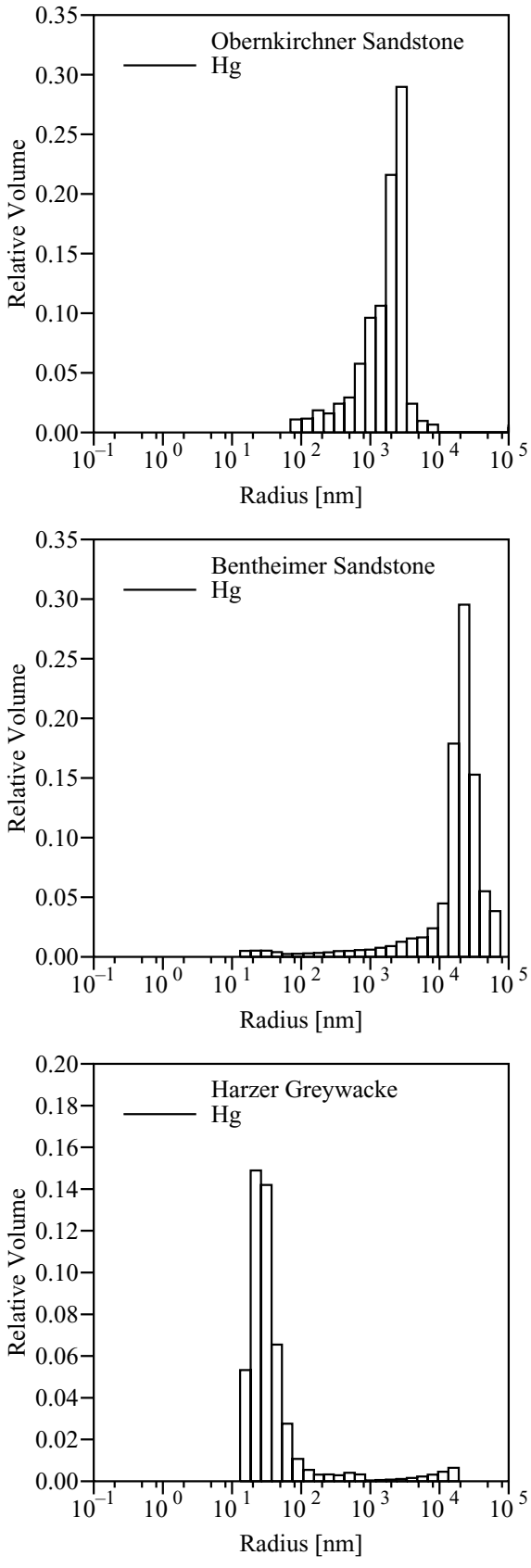

Figure 5. Pore radius distribution, determined with mercury (Hg) of Obernkirchner Sandstone (top: OK) after Schopper & Riepe (1986), of Bentheimer Sandstone (middle: BH) and Harzer Greywacke (bottom: HZ) after Sellmann (1990).

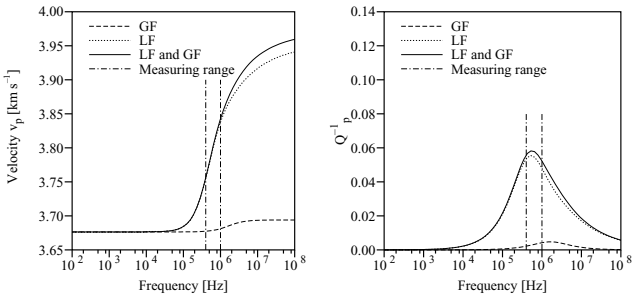

Figure 6. Velocity v_p and attenuation $1/Q$ vs frequency, calculated for Obernkirchner Sandstone (31 per cent water saturation) using three different models: GF—global fluid flow, LF—local fluid flow, LF and GF—combined model. Due to the fact that *P* and *S* waves are influenced in a similar way, only the *P* wave is shown. Model parameters are listed in Tables 2, 3 and 4. In the frequency range of ultrasonic measurements (indicated by vertical lines) a strong influence of both relaxation mechanisms has to be stated.

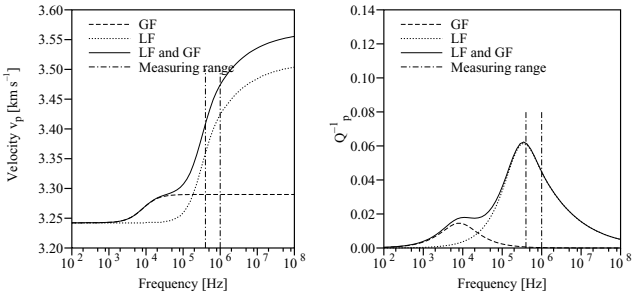

Figure 7. Like Fig. 6 for Bentheimer Sandstone (53 per cent water saturation). The *P*-wave velocity in ultrasonic range is increased due to GF.

describing the effect of the GF and LF are solved analogous to Biot (1956) (see Appendix A). As a result the velocities and attenuations of seismic waves in saturated sandstones can be calculated as a function of macroscopically determined parameters (porosity and permeability) as well as of microscopic parameters (dimension, geometry, density of microcracks and the constitution of grain contacts). The combined model contains the Gassmann model, included in the equations of Biot (1956).

3.2 Determination of the parameters

In general the parameters for the GF model can easily be obtained by direct measurements (see Table 2). The parameters for the LF model have to be derived from various data. The bulk and shear moduli (K_b and N), describing the elastic behaviour of grain contacts, are obtained from the measured velocities v_p and v_s in dry rock. The mean radius of the grains R and the length of cracks $l = 2a$ are determined by analysis of thin sections (Figs 2, 3 and 4). The radius of the torus b and the height of the microcracks h are obtained from measurements of pore radius distribution with mercury (Fig. 5) and nitrogen. The aspect ratio h/a is additionally verified by modelling of the ultrasonic measurements dependent on saturation (see Section 3.5). Furthermore, the modelling yields the amount of the modulus reduction and the distribution of the fluid in the rock. The crack density γ can be estimated from thin sections or by matching measurements. In this work the latter is chosen.

3.3 Influence of fluid flow in ultrasonic range

In order to get an estimation about the influence of the two frequency-dependent fluid flow mechanisms in the ultrasonic range the frequency dependence of velocity and attenuation $1/Q$ for both, the GF and the LF, are shown for the three rock types under investigation (Figs 6–8). The parameters used for the calculations are given in Tables 2, 3 and 4.

In the high-porosity Obernkirchner Sandstone (porosity = 18.5 per cent) the effect of the GF is smaller than the effect of the LF (Fig. 6). For water the relaxation frequencies of the two fluid flow models are nearly the same, thus they cannot be seen separately. Because they are located within the ultrasonic range (approx. 0.4–1 MHz), the velocities and attenuations in saturated rock are increased due to both mechanisms.

In Bentheimer Sandstone (porosity = 23.2 per cent), the relaxation frequency of the LF f_{LF} is approximately the same as for Obernkirchner Sandstone, whereas the relaxation frequency of the GF f_{GF} is shifted towards lower frequencies (Fig. 7). For this reason

Table 2. Model parameters for the individual rocks (Mayr 2002).

Parameter	Symbol [unit]	Obernkirchner Sandstone	Bentheimer Sandstone	Harzer Greywacke
Density of matrix material	ρ_s [kg/m^3]	2.657	2.643	2.683
Porosity	ϕ	0.185	0.232	0.018
irreducible water saturation	Sw_{red} [per cent]	9	10	100
for frequency and pressure-dependent calculations:				
saturation	S_w [per cent]	31	53	73
for frequency and saturation-dependent calculations:				
v_p in dry rock	v_{dry} [km s^{-1}]	3.8	3.48	5.14
v_s in dry rock	v_{dry} [km s^{-1}]	2.37	2.13	3.28
Additional: LF model				
Meanradius	R [μm]	55	110	90
Radius of torus	b [μm]	2	22	0.035
Slit height	h [nm]	70	110	7
Slit lenght	a [μm]	40	77	63.5
Rel. slitvolume	S_s [per cent]	9.6	0.2	98
for saturation-dependent calculations:				
Crack density	γ [-]	0.006	0.005	0.001
Additional: GF model				
Permeability	κ [10^{-15} m^2]	9	2.3×10^3	20×10^{-5}

Table 3. Common parameters used for calculations of global (GF) and local fluid flow (LF), (Wulff 1995).

Parameter	Model	Symbol[unit]	Value
Number of grain–grain contacts	LF	μ	9
Bulk modulus of matrix material	LF	K_s[GPa]	38
Structural parameter, Tortuosity	GF	δ	$\sqrt{8}$
Coupling parameter	GF	α'	2

Table 4. The parameters of pores' fillings (Wulff 1995).

Pores' filling		Water	Air
Bulk modulus	K_f [GPa]	2.19	8×10^{-3}
Viscosity	$\eta[\frac{10^{-3}\,\mathrm{Ns}}{\mathrm{m}^2}]$	1.0	0
Density	ρ_f[kg m^{-3}]	1000	1.1×10^{-3}

the velocities are increased and the waves are hardly attenuated due to the GF in the ultrasonic range. The LF will lead to increased velocities and attenuations.

In the case of the Harzer Greywacke (porosity = 1.5 per cent) f_{GF} is shifted towards higher frequencies ($>10^8$ Hz). For this reason the GF has no influence in the measuring range. The relaxation frequency f_{LF} shifts towards lower frequencies, therefore the velocities are increased due to the LF in the ultrasonic range and the waves are hardly attenuated there (Fig. 8).

In the combined model the effect of both types of flow superimpose linearly (Figs 6–8). For Bentheimer Sandstone and Harzer Greywacke the linear superimposing is more obvious than for Obernkirchner Sandstone.

3.4 Implementation of saturation dependence

Homogeneous and inhomogeneous (gas pockets) saturation is included in the model. In both cases, it is assumed that small microcracks (represented by the slits) are filled first (Mavko & Noelen-Hoeksema 1994; Murphy *et al.* 1986). All slits are fully saturated at the saturation S_s, and the behaviour is characterised only by the LF and there is no GF, *cf.* Figs 9 and 10. Thus in the range of $0 < S_w < S_s$, the saturation for the GF S_w^* is set to 0. Above S_s, the total saturation S_w is a combination of the saturation S_s and the fraction of the saturation of the pores (represented by the torus) $S_w^*\,(1 - S_s)$:

$$S_w = S_s + S_w^*(1 - S_s). \tag{3}$$

This means that in the range of $S_w > S_s$, the GF has an additional effect on the seismic waves.

In case of homogeneous gas–fluid mixture, at saturations higher than S_s the fraction S_w^* leads to GF, *cf.* Fig. 9. In all models—using homogeneous mixture—the influence of the increasing density can

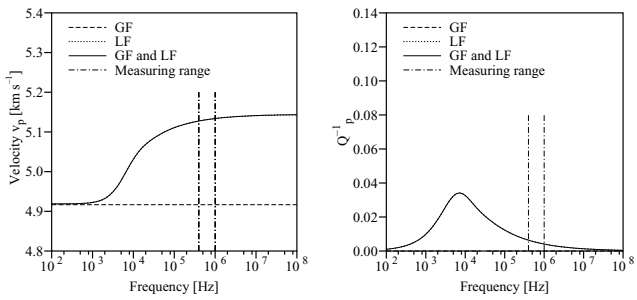

Figure 8. Like Fig. 6 for Harzer Greywacke (73 per cent water saturation). The influence of global fluid flow is small.

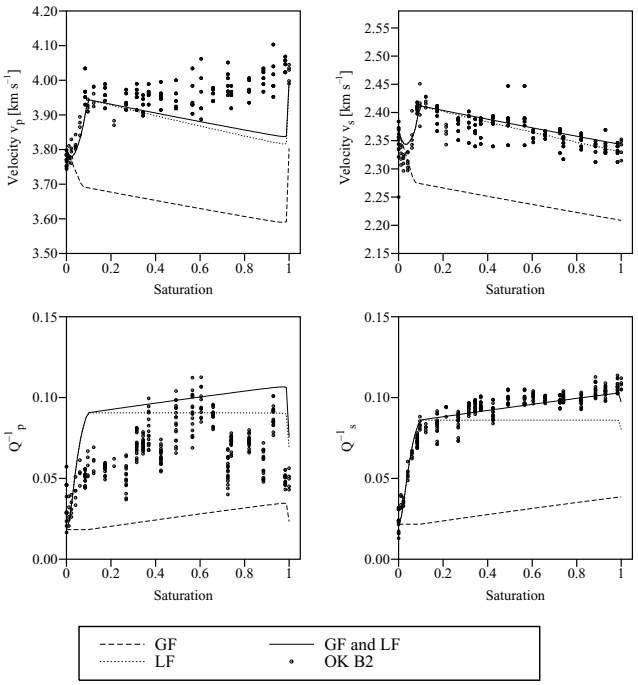

Figure 9. Comparison of theoretical dependence on saturation of the global (GF), local fluid flow (LF) and the combined model (GF and LF) under the assumption of a homogeneous gas–fluid mixture with measurements (uniaxial pressure = 30 MPa) on Obernkirchner Sandstone (OK). Frequency: 1 MHz, $m_{\mathrm{red0}}\,p = 5$ per cent, $m_{\mathrm{red0}}\,s = 7$ per cent. For other parameters see Tables 2, 3 and 4. GF leads to an underestimation of the data, the LF and the combined model with both GF and LF reproduce attenuation and velocity of the *S* waves. Data: after Schütt (1992).

be seen. The attenuations calculated with the LF model stay constant with increasing saturation, while those calculated with the combined model are increasing due to the GF. At full saturation the attenuation of both waves, calculated with the LF model and the combined model, respectively, is slightly decreased because the torus is fully saturated with fluid having a high compression modulus compared to gas, thus the LF is inhibited. The *P* velocity additionally increases at full saturation in all models due to the Gassmann effect while at the same time the attenuation is decreasing.

In the gas-packet model the moduli (M_{GP}, N_{GP}) above the saturation S_s are obtained by calculating a mean value after Voigt (e.g. Mavko *et al.* 1998). In these calculations the used moduli are an average of the moduli found in a region were only LF is effective $M_{LF}^{(S_w=S_s)}$ and a fully saturated area, influenced by both kinds of fluid flow $M_{LGF}^{(S_w=1)}$:

$$\begin{aligned} M_{GP} &= S_w^* M_{LGF}^{(S_w=1)} + \left(1 - S_w^*\right) M_{LF}^{(S_w=S_s)}, \\ N_{GP} &= S_w^* N_{LGF}^{(S_w=1)} + \left(1 - S_w^*\right) N_{LF}^{(S_w=S_s)}, \end{aligned} \tag{4}$$

with

$$M = v_p^2 \cdot \rho,\ N = v_s^2 \cdot \rho,$$

ρ = density of saturated rock.

Because the Gassmann effect is included in calculating M_{GP}, it becomes more and more effective in the range of $S_s < S_w < 1$, *cf.* Fig. 10. The gas-packet model can be looked upon as an upper bound and the homogeneous gas–fluid mixture as a lower bound for the effective moduli. The effect of the modulus reduction is included in the model in a phenomenological way as introduced by, for example,

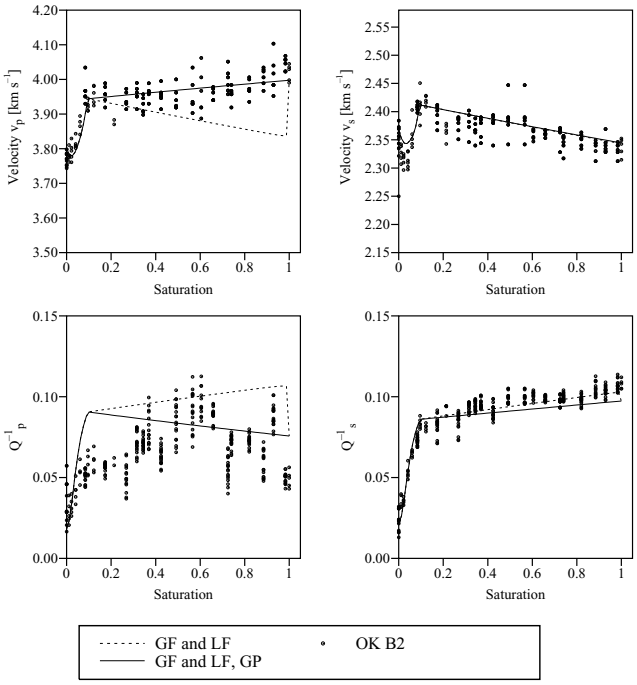

Figure 10. Like Fig. 9, but comparison between combined model with homogeneous mixture (GF and LF), respectively, combined model with gas pockets (GF and LF, GP) and data. With the latter one the adjustment of the data succeeds.

Mörig (1993) and Wulff (1996):

$$v^2_{\text{partsat}} = v^2_{\text{dry}}(1 - m_{\text{red0}}). \tag{5}$$

The modulus reduction m_{red} is constant for saturations above a certain value $S_{w\,\text{red}}$, typical for each rock. This saturation depends on the irreducible water saturation and has to be determined by experiments. For saturations S_w below $S_{w\,\text{red}}$ the following m_{red} has to be used:

$$m_{\text{red}} = m_{\text{red0}} \frac{S_w}{S_{w\,\text{red}}}. \tag{6}$$

For P and S waves different values, $m_{\text{red0}\,p}$ and $m_{\text{red0}\,s}$, respectively, can occur (Mörig 1993; King *et al.* 2000).

3.5 Modelling of saturation dependence

The comparison between the calculated and measured data for Obernkirchner Sandstone shows that with the model of GF neither the velocity nor the attenuation can be fitted (Fig. 9, data are taken from Schütt 1992). With the LF model only a restricted fitting can be achieved with P-wave velocities and S-wave attenuations being underestimated for saturations higher than 50 per cent. Assuming homogenous saturation and making use of the combined model, the same result is yielded for the P-wave velocities. By this approach the S-wave attenuation can be fitted well. By taking inhomogeneous saturation (gas pockets) and both types of fluid flow into account, the increase in the P-wave velocities with saturation due to the Gassmann effect is smeared over a wide range of saturation. As a result, the velocities and attenuations of the P waves can be fitted better (Fig. 10). For the S waves there is no significant difference between the two saturation models. The crack density γ and the modulus reduction were chosen to achieve a satisfactory fit of velocities and attenuations at saturations between 40 and 60 per cent. The modulus reduction for S waves had to be set higher than for P waves. This is in agreement with the increasing v_p/v_s-ratio for increasing saturation, observed by Mörig (1993) in the seismic range.

For the Bentheimer Sandstone similar observations have been made. In case of the Harzer Greywacke the data can be explained with only LF.

The parameters obtained for the rocks are given in Tables 2 and 3.

3.6 Implementation of pressure dependence

The changing strength of the grain contacts with pressure is included in the model by using the velocities in the dry rocks, measured as a function of pressure. The increase in velocities in dry rocks with hydrostatic pressure leads to

(i) an increase in the calculated velocities in saturated rock and
(ii) a decrease in attenuation.

Only the attenuation due to the fluid (i.e. the difference between attenuation measured in saturated rock $\frac{1}{Q_{\text{sat}}}$ and in dry rock $\frac{1}{Q_{\text{dry}}}$) is used for fitting. In doing so, the pressure-dependent change of elastic and inelastic properties of the grain contacts in dry rocks are removed. Thus they do not have to be included explicitly in the model.

The pressure induced reduction of the influence of the LF, and by this of the microstructure, on the velocities and attenuations is modelled by variation of the pressure dependence of the crack density γ. A crack density function was introduced for this purpose:

$$\gamma = (\gamma_0 - \gamma^*)e^{-P_c/P^*} + \gamma^*,$$

where γ_0 is the crack density at low pressure (p_0), γ^* is the part of non-closable microcracks, P_c is the confining hydrostatic pressure and P^* is the pressure at which the part of closable cracks ($\gamma_0 - \gamma^*$) is reduced by $1/e$.

With this approach an exponential closure of cracks can be described, as proposed by, for example, Johnston *et al.* (1979) and theoretically derived by Shapiro (2003). The relation between the crack density and the variation of elastic moduli is emphasised (see Zimmerman 1991). The elastic moduli and velocities are often related to pressure by an exponential law, for example, Zimmerman *et al.* (1986), Prasad & Manghnani (1997). Furthermore, it is taken into consideration that the rocks contain cracks, which cannot be closed by hydrostatic pressure because they are kept open by, for example, small spikes at the surface of the crack, that is, the roughness of crack surface.

The parameters velocity v_{dry} and crack density γ have the most significant influence on the velocities and attenuation in saturated rocks, (Mayr 2002). The change of less significant parameters are also considered: Reducing the height h leads, in case of the used high-porosity rocks ($f \approx f_{LF}$), to an increase in the attenuation, but the velocities remain constant in the ultrasonic range (Fig. 11). Reduction of permeability and porosity leads to a negligible decrease in the velocities. The modulus reductions are considered as independent of pressure, (Wulff & Burkhardt 1997).

4 PRESSURE DEPENDENCE: EXPERIMENTAL RESULTS

4.1 Velocities

In the vacuum dry as well as in the partially water saturated high-porosity *Obernkirchner Sandstone*, the increase in velocities is non-linear with pressure up to approximately 60 MPa. Above this

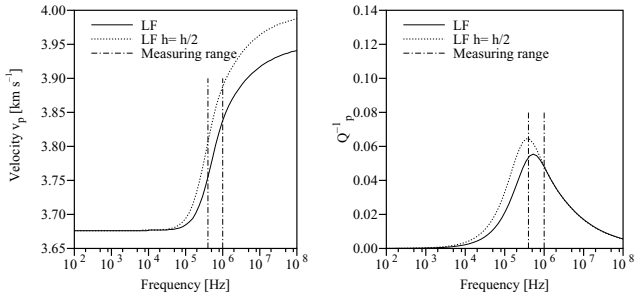

Figure 11. Like Fig. 6 but influence of slit height h on LF response.

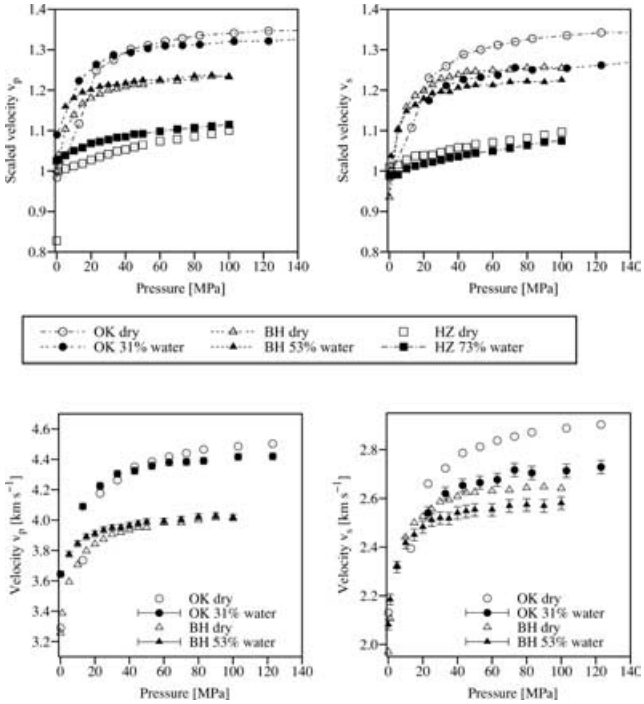

Figure 12. *P*- and *S*-wave velocities of Obernkirchner Sandstone (OK), Bentheimer Sandstone (BH) and Harzer Greywacke (HZ), dry and water saturated (31 per cent, 53 per cent, 73 per cent, respectively). To compare the change of velocities with pressure, the axes for *P* and *S* waves are scaled with a constant ratio between maximum and minimum value with respect to the mean $[(v_{max} - v_{min})/v_{mean}]$. Bars indicate error of measurement.

pressure the increase is approximately proportional to the pressure (Fig. 12). The total increase of the velocity in the dry rock is ≈35 per cent/100 MPa. By partial saturation, the velocity of the *P* wave increases at low hydrostatic pressure, while the velocity of the *S* wave is hardly changed. The increase in the velocities with pressure measured in the partially saturated rock is less than in the dry rock. This is due to the effect of LF being reduced by hydrostatic pressure (*cf.* Section 5.1).

In the dry *Bentheimer Sandstone* the increase of the velocities is less than in the Obernkirchner Sandstone (≈20 per cent/100 MPa). Here a linear increase in velocities can be observed above approximately 40 MPa (Fig. 12). By partial saturation, the velocity of the *P* wave increases at low hydrostatic pressure, while the velocity of the *S* wave is hardly changed in this sandstone, too. Above a hydrostatic pressure of 40 MPa the velocities of the *P* wave in vacuum dry and partially saturated rock are similar within the range

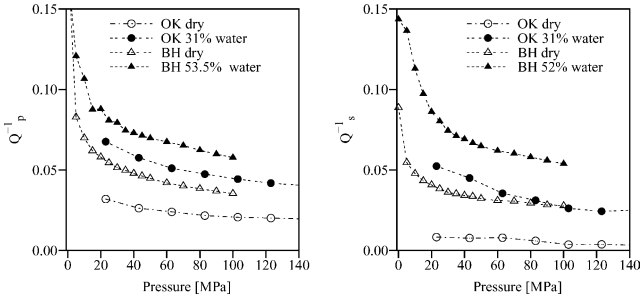

Figure 13. Like Fig. 12 but *P*- and *S*-wave attenuations $1/Q$ of Obernkirchner Sandstone (OK), Bentheimer Sandstone (BH).

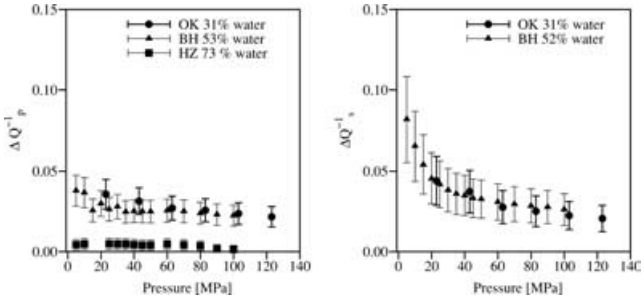

Figure 14. Like Fig. 12 but *P*- and *S*-wave attenuations due to fluid flow: $\Delta\ 1/Q = 1/Q_{sat} - 1/Q_{dry}$.

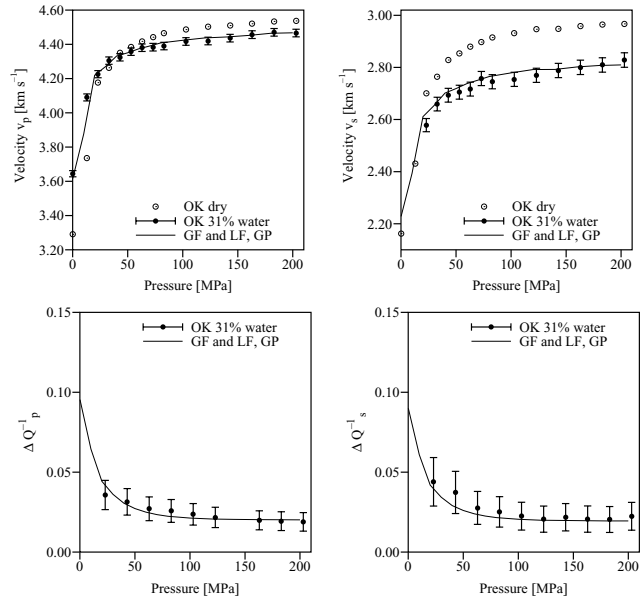

Figure 15. Measured *P*- and *S*-wave velocities and attenuations ($\frac{1}{Q_{sat}} - \frac{1}{Q_{dry}}$) of Obernkirchner Sandstone (OK), partial water saturation (31 per cent), and results of modelling with combined model under the assumption of gas pockets (GF and LF, GP): crack density at low pressure: $\gamma_0 = 0$, 007; crack density at high pressure: $\gamma^* = 0$, 002; $\frac{\gamma_0 - \gamma^*}{\gamma_0} = 0.71$; $P^* = 25$ MPa, m_{red0} $p = 5$ per cent, m_{red0} $s = 8$ per cent. For other parameters see Tables 2, 3 and 4.

of the error (Fig. 12). The velocity of the *S* wave in the partially saturated Bentheimer Sandstone is always smaller than in the dry one. This indicates a different change of the microstructure by the pressure (*cf.* Section 5.2).

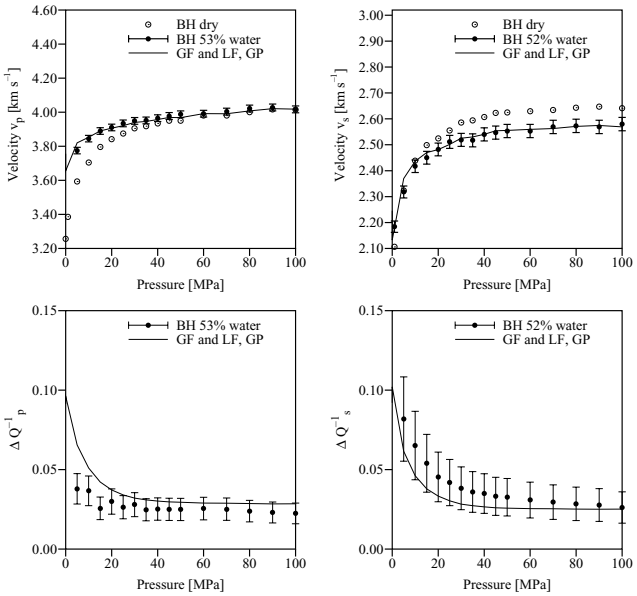

Figure 16. Like Fig. 15 for Bentheimer Sandstone (BH), partial water saturation (53 per cent), modelling with combined model under the assumption of gas pockets (GF and LF, GP): $\gamma_0 = 0,007$; $\gamma^* = 0,0025$; $\frac{\gamma_0 - \gamma^*}{\gamma_0} = 0.64$; $P^* = 10$ MPa, $m_{\mathrm{red0}} p = 8$ per cent, $m_{\mathrm{red0}} s = 8$ per cent.

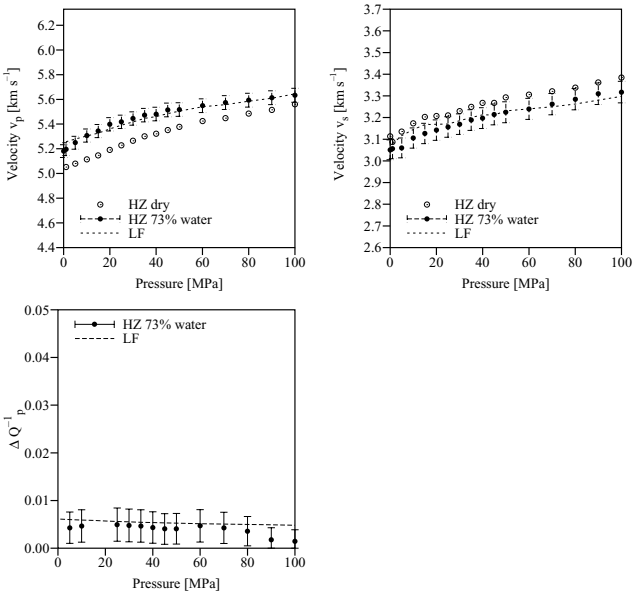

Figure 17. Like Fig. 15 for Harzer Greywacke (HZ), partial water saturation (73 per cent), modelling with local fluid flow model (LF): $\gamma_0 = 0,00105$; $\gamma^* = 0,0009$; $\frac{\gamma_0 - \gamma^*}{\gamma_0} = 0.17$; $P^* = 100$ MPa, $m_{\mathrm{red0}} p = 17$ per cent, $m_{\mathrm{red0}} s = 26$ per cent.

In both high-porosity sandstones the non-linear increase in velocities with pressure in dry rocks indicates an increase in the strength of the grain contacts due to the closure of microcracks. In Obernkirchner Sandstone these cracks are closed at a higher pressure than in Bentheimer Sandstone (approx. 60 and 40 MPa, respectively). Above this closure pressure it is assumed that no more cracks can be closed, the increase in the strength of the grain contacts (leading to the linear increase in velocities with pressure) is only due to the higher normal force on the contacts. Different amounts of increase in velocities with pressure indicate that in Bentheimer Sandstone less cracks can be closed by hydrostatic pressure than in Obernkirchner Sandstone. The different amounts of increase of the velocities in dry and saturated sandstones with pressure indicate a decreasing influence of fluid flow on the seismic attributes.

In the *Harzer Greywacke*, a much lower (approx. 10 per cent/100 MPa) and less non-linear increase in velocities with increasing pressure is observed, compared to the high-porosity sandstones (Fig. 12). In this rock the velocity of the P wave in the partially saturated rock is always higher and of the S wave always smaller than in the dry one (*cf.* Section 3.5). This implies that less cracks can be closed and the range of pressure in which they are closed might be higher than in the high-porosity sandstones (*cf.* Section 5.3).

4.2 Attenuation

The attenuation $\frac{1}{Q}$ of both types of waves in dry and in partially water saturated Bentheimer Sandstone is in general slightly higher than in Obernkirchner Sandstone (Fig. 13). This may be due to different amounts of scattering, because the mean grain radius in Bentheimer Sandstone ($R_{\mathrm{mean}} = 0.11\,10^{-3}$ m) is greater than in Obernkirchner Sandstone ($R_{\mathrm{mean}} = 0.055\,10^{-3}$ m), *cf.* Figs 2 and 3. The mean wavelength for P waves and S waves are: $\lambda_p \approx 3.5\,10^{-3}$ m, $\lambda_s \approx 2.5\,10^{-3}$ m. The attenuation of the P wave in dry and in water saturated Harzer Greywacke is much lower than in the other Sandstones.

In the two dry sandstones, the decrease in attenuation is approximately linear with pressure above 60 MPa for Obernkirchner and 40 MPa for Bentheimer Sandstone (see Fig. 13). This can be explained by the fact that after the closure of cracks friction at grain contacts is still decreasing in this region due to the increasing normal force on the contacts.

The increase in the attenuations for both types of waves due to saturation ($\Delta \frac{1}{Q} = \frac{1}{Q_{\mathrm{sat}}} - \frac{1}{Q_{\mathrm{dry}}}$)—being nearly the same for Obernkirchner and Bentheimer Sandstone—are becoming smaller with increasing pressure (Fig. 14). In both rocks the increase due to saturation can be seen even at an effective hydrostatic pressure above 60 MPa. This indicates that the influence of fluid flow is decreasing with increasing pressure but has still a measurable effect above 60 MPa. The $\Delta \frac{1}{Q_p}$ in the Harzer Greywacke is much lower than in the other Sandstones and is constant within the range of error (Fig. 14). This means that in this rock the fluid flow effects are nearly constant and less than in the other sandstones.

5 PRESSURE DEPENDENCE: MODELLING AND DISCUSSION

For modelling the dependence of the measured attenuations and velocities in the partially saturated sandstones the parameters obtained in Section 3.2 and the conditions outlined in Section 3.6 are used. The inhomogeneous saturation (gas-pocket model) and both fluid flow mechanisms are used as this combined model fits the data at various saturations best (see Section 3.5).

5.1 Obernkirchner sandstone

At low hydrostatic pressures the increase in velocities and attenuations measured in partially water saturated (31 per cent) Obernkirchner Sandstone can be explained by fluid flow, mainly LF in the cracks combined with GF and inhomogeneous saturation (Fig. 15). Using the combined model yields modulus reductions comparable to those obtained for the uniaxial measurements. The crack density γ_0 had

to be chosen greater than the one obtained by modelling the measurements at different degrees of saturation (Table 2). This can be explained by the fact that Schütt (1992) did these measurements at a higher uniaxial stress (≈30 MPa compared to ≈3.5 MPa) and thereby some cracks have been closed in the sandstones leading to a lower influence in the LF contribution on the seismic attributes. The increasing velocities with increasing pressure are attributed to a decreasing influence of LF. Pressure P^* (see Section 3.6) had to be set to 25 MPa to achieve a satisfying fit for all data. This means that at 25 MPa the density of closable cracks is reduced by $1/e$. At higher pressures the velocities measured in partially saturated sandstones are lower than the ones in dry sandstone. This can be explained by both the higher density and the reduction in modulus in partially saturated rock. However, it is necessary to take the LF into consideration to explain both the velocities and the attenuations at high pressures. The modelling yields that ≈70 per cent of the cracks can be closed by the applied hydrostatic pressure.

5.2 Bentheimer sandstone

In the partially water saturated (53 per cent) Bentheimer Sandstone, the model demonstrates that there is again a considerable closure of cracks by pressure (Fig. 16), similar to Obernkirchner Sandstone. Here a lower pressure P^* had to be chosen (10 MPa) to achieve a good fit for all data, especially for the velocities and attenuations of *P* waves. This is comparable to the phenomenological interpretation. The modelling yields that only ≈60 per cent of the cracks are closed at maximum measuring pressure, analogous to Section 4, where a less effective closure of cracks than in the Obernkirchner Sandstone was predicted.

5.3 Harzer Greywacke

The Harzer Greywacke, with 73 per cent water saturation, shows a clearly different behaviour. At low pressure there are less cracks than in the sandstones (Fig. 17). The pressure P^* had to be set higher (100 MPa), the amount of closable cracks is only ≈14 per cent. Again this is comparable to the phenomenological interpretation.

6 FURTHER DISCUSSIONS

The experimental data can be fitted, within the error bars, with the combined model, that is, taking into account the GF (Biot 1956) and the LF (Murphy *et al.* 1986) and assuming an inhomogeneous fluid distribution in the sandstones (Figs 15 and 16). However, still there are some remaining questions which are discussed below.

6.1 Attenuation of *S* wave

In both sandstones the attenuation of the *S* wave decreases less with pressure than the one of the *P* wave and as predicted by the modelling. The following possible effects may lead to an additional attenuation of the *S* waves:

It may be assumed that the attenuation of *P* waves is less influenced by LF than that of *S* waves. However, in the vicinity of the relaxation frequency, LF is leading to both an increase in velocities and in attenuation, similar for both waves. Due to the fact that the velocities have been fitted over the whole pressure range a different influence of LF on *S* and *P* waves is implausible.

Furthermore, friction at grain contacts could be taken into account, as described by Tao *et al.* (1995) and by Johnston *et al.* (1979). On the other hand measurements on Obernkirchner Sandstone, saturated with non-polar fluids (e.g. cyclohexane and fluid paraffin), are showing the same behaviour, (*cf.* Mayr 2002). Therefore, it must be clarified, why non-polar fluids are changing the friction in a similar way like polar fluids.

Additionally, scattering of seismic waves could be influenced by the fluids. For the explanation of the pressure dependence of this effect, the reflection coefficient must be seen as varying with pressure. This could be due to the squeezing out of the wetting fluid in the cracks.

6.2 Mean values of radii and heights

For the modelling of the data only mean values for the parameters grain and pore radii (for determination of torus radius *b* and slit heights *h*) are used, although these parameters have a broad variety (Schopper & Riepe 1986; Schopper *et al.* 1990; Sellmann 1990). The use of mean parameters is justified by the facts that

(i) the saturation-dependent measurements can be fitted with the mean parameters, and

(ii) using more parameters to describe the pore structure (*h* and *b*) only leads to more free parameters, but does not reveal additional information about the closure of cracks (*cf.* Wulff & Burkhardt 1997).

7 CONCLUSIONS AND SUMMARY

In this paper a new combined model is presented. It includes global fluid flow and local fluid flow (LF), in combination with the Gassmann effect and modulus reduction. In addition two different distributions (homogeneous and inhomogeneous) of the fluid in the partially saturated rock can be modelled. Most parameters, used for the description of the microstructure, can be determined by petrophysical measurements. The other parameters (i.e. crack density γ and modulus reduction mod_{red}) can be obtained by modelling measurements at low uniaxial stress as a function of saturation. The results obtained using the parameters γ and mod_{red} give a good fit to the saturation-dependent data. Together with measurements the combined model with a mean aspect ratio provides a reasonable approximation to be used as a tool for the investigation of the closure of cracks in sandstones. The influence of the Gassmann effect and an inhomogeneous fluid distribution (gas pockets) models well the saturation dependence of the *P*-wave velocities. Thus modelling as a function of pressure will reveal a reliable crack density function.

The phenomenological interpretation and the results of the modelling are in agreement with respect to the amount and range of crack closure. The different increase in velocity with pressure in the Obernkirchner and Bentheimer Sandstone can be explained by a different amount of crack closure. In contrast to the sandstones, the modelling shows that in Harzer Greywacke there are fewer cracks at low pressure. In this rock less cracks can be closed by hydrostatic pressure and a much higher pressure is necessary to close them. The different behaviour of the attenuation of *S* waves can be seen as a minor effect.

Finally it can be concluded that there must be open cracks in all rocks under elevated hydrostatic pressure, leading to a measurable effect due to the LF. These considerations must be taken into account when transferring velocities and attenuations from measurements in the laboratory, performed at low pressure, to higher pressures as found *in situ* and from ultrasonic frequency range into sonic or seismic frequency range.

ACKNOWLEDGMENTS

We thank the colleagues of the Department of Geophysics, Technical University Berlin, for their support during the experiments and their helpful discussions. We particularly thank C. von Engelhardt and S. Stöver for preparation of the thin sections as well as R. Schütt for providing the data of his saturation-dependent measurements, W. Debschütz for the data of pore radius distribution and two anonymous reviewers for useful comments and suggestions, which helped to improve the paper.

REFERENCES

Berryman, J., 1980. Confirmation of Biot's Theory, *Appl. Phys. Lett.,* **37,** 382–384.

Berryman, J.G., 1988. Seismic wave attenuation in fluid-saturated porous media, *Pageoph,* **128,** 423–432.

Biot, M.A., 1956. Theory of propagation of elastic waves in a fluid-saturated porous solid.I. Low-frequency range, *J. acoust. Soc. Am.,* **28,** 168–178.

Biot, M.A. & Willis, D.G., 1957. The elastic coefficients of the theory of consolidation, *J. Appl. Mech.,* **24,** 594–601.

Bourbié, T., Coussy, O. & Zinszner, B., 1987. *Acoustics of porous media*, Édition Technip, Paris.

Burkhardt, H., Paffenholz, J. & Schütt, R., 1986. Measurements of *Q* on natural rock samples in different frequency ranges, in *Absorption of seismic waves*, DGMK-Projekt 254, 203–238, German Soc. for Petroleum Sciences and Coal Chemistry, Hamburg.

Burkhardt, H., Mörig, R. & Schütt R., 1990. Experimental and theoretical investigations of seismic wave absorption mechanisms in sedimentary rocks, in *Application of Absorption of Seismic Waves in Hydrocarbon Exploration*, DGMK-report 386, 141–199, German Soc. for Petroleum Sciences and Coal Chemistry, Hamburg.

Burkhardt, H., Mörig, R. & Schütt R., 1992. Laboratory investigations on rock samples to establish further fundamentals for the lithological interpretation of seismic measurements, in *Evaluation of Lithologic Parameters in Hydrocarbon Reservoirs by Simultaneous Application of Compressional and Shear Waves*, DGMK-report 397, 241–279, German Soc. for Petroleum Sciences and Coal Chemistry, Hamburg.

Cadoret, T., Marion, D. & Zinszner, B., 1995. Influence of frequency and fluid distribution on elastic wave velocities in partially saturated limestones, *J. geophys. Res.,* **100,** 882–894.

Cadoret, T., Mavko, G. & Zinszner, B., 1998. Fluid distribution effect on sonic attenuation in partially saturated limestones, *Geophysics,* **63,** 154–160.

Diallo, M.S., Prasad, M. & Appel, E., 2003. Comparison between experimental results and theoretical predictions for P-wave velocity and attenuation at ultrasonic frequency, *Wave motion,* **37,** 1–16.

Dvorkin, J. & Nur, A., 1993. Dynamic poroelasticity: a unified model with the squirt and the Biot mechanisms, *Geophysics,* **58,** 524–533.

Freund, D., 1992. Ultrasonic compressional and shear velocities in dry clastic rocks as a function of porosity, clay content, and confining pressure, *Geophys. J. Int.,* **108,** 125–135.

Gassmann, F., 1951. Über die Elastizität poröser Medien, *Vierteljahresschrift d. Naturf. Ges. Zürich,* **96,** 1–23.

Johnson, K.L., Kendall, K. & Roberts, A.D., 1971. Surface energy and the contact of elastic solids, *Proc. Roy. Soc.,* **324,** 301–313.

Johnston, D.H., Toksöz, M.N. & Timur A., 1979. Attenuation of seismic waves in dry and saturated rocks: II Mechanisms, *Geophysics,* **44,** 691–711.

King M.S., 1966. Wave velocities in rocks as a function of changes in overburden pressure and pore fluid saturants, *Geophysics,* **31,** 50–73.

King, M.S., Marsden, J.R. & Dennis J.W., 2000. Biot dispersion for P- and S-wave velocities in partially and fully saturated sandstones, *Geophys. Prospect.,* **48,** 1075–1089.

Koesoemadinata, A.P. & McMechan, G.A., 2001. Empirical estimation of viscoelastic seismic parameters from petrophysical properties of sandstone. *Geophysics,* **66,** 1340–1649.

Knight, R. & Nolen-Hoeksema, R., 1990. A laboratory study of the dependence of elastic wave velocities on pore scale fluid distribution, *Geophys. Res. lett.,* **17,** 1529–1532.

Knight, R., Dvorkin, J. & Nur, A., 1998. Acoustic signatures of partial saturation, *Geophysics,* **63,** 132–138.

Lebedev, E.B., Ryzhenko, B.N., Dorfman, A.M., Zebrin, S.R., Sokolova, N.T., Burkhardt, H., Mörig, R. & Wulff A.-M., 1996. Influence of fluids on the elastic properties of sandstone at high pressure and temperature, *Geophys. Res. Lett.,* **23,** 3115–3118.

Mavko, G. & Jizba, D., 1991. Estimating grain-scale fluid effects on velocity dispersion in rocks, *Geophysics,* **56,** 1940–1949.

Mavko, G. & Noelen-Hoeksema, R., 1994. Estimating seismic velocities at ultrasonic frequencies in partial saturated rocks, *Geophysics,* **59,** 252–258.

Mavko, G., Mukerji, T. & Dvorkin, J., 1998. *The rock physics handbook: tools for seismic analysis in porous media.* Cambridge University Press, New York.

Mayr, S.I., 2002. Der Einfluss der Mikrostruktur auf die Ultraschalleigenschaften von Sandsteinen bei hydrostatischen Druckbedingungen, (The influence of the microstructure on the ultrasonic behaviour of sandstones under hydrostatic pressure) *PhD thesis*, Technical University of Berlin, Berlin.

Mayr, S.I. & Burkhardt, H., 2002, Ultraschallmessungen zur Untersuchung der Veränderung der Mikrostruktur von Sandsteinen bei hydrostatischen Druckbedingungen, *DGG-Mitteilungen,* DGG-Sonderband: FKPE-Tagung 2001.

Mörig, R., 1993. Zusammenhang von seismischen und lithologischen Parametern sedimentärer Festgesteine, *PhD thesis*, Technical University of Berlin, Berlin.

Murphy, W.F. III, 1982. Effects of partial water saturation on attenuation in Massilon sandstone and Vycor porous glass, *J. acoust. Soc. Am.,* **71,** 1458–1468.

Murphy, W.F. III, 1984. Acoustic measures of partial gas saturation in tight sandstones, *J. geophys. Res.,* **89,** 11 549–11 559.

Murphy, W.F. III, Winkler, K.W. & Kleinberg, R.L., 1986. Acoustic relaxation in sedimentary rocks: dependence on grain contact and fluid saturation, *Geophysics,* **51,** 757–766.

Parra, J.O., 1997. The transversly isotropic poroelastic wave equation including the Biot and the squirt mechanisms: theory and application, *Geophysics,* **62,** 302–318.

Prasad, M. & Manghnani, M.H., 1997. Effects of pore and differential pressure on compressional Wave velocity and quality factor in Berea and Michigan sandstones, *Geophysics,* **62,** 1163–1176.

Schön, J., 1983. *Petrophysik*, Ferdinand Enke Verlag, Stuttgart.

Schön, J., 1997. *Physical Properties of Rocks: Fundamentals and Principles of Petrophysics*, H.G.E, **28,** Elsevier, Amsterdam.

Schopper, J.R. & Riepe, L., 1986. Experimental und theoretical petrophysical investigations on relations between the inelastic absorption in porous rocks and other petrophysical and reservoir parameters, in *Absorption of seismic waves*, DGMK-Projekt 254, 200–246, German Soc. for Petroleum Sciences and Coal Chemistry, Hamburg.

Schopper, J.R., Debschütz, W. & Kulenkampff, J., 1990. Lithological Interpretation of ASW-Mechanisms by Petrophysical Measurements and Logging Data, in *Application of Absorption of Seismic Waves in Hydrocarbon Exploration*, DGMK-report 386, 232–276, German Soc. for Petroleum Sciences and Coal Chemistry, Hamburg.

Schütt, R., 1992. Experimentelle und theoretische Untersuchungen zur Dämpfung und Geschwindigkeiten von Kompressions- und Scherwellen in Sedimentgesteinen bei Ultraschallfrequenzen, *PhD thesis*, Technical University of Berlin, Berlin.

Shapiro, S.A., 2003. Elastic piezosensitivity of porous and fractured rocks. *Geophysics,* **68,** 482–486.

Sellmann, C, 1990. Bestimmung der vollständigen Porenradienverteilung natürlicher Gesteine, *Diplom-Arbeit,* Technical University Clausthal.

Tao, G., King, M.S. & Nabi-Bidhendi M., 1995. Ultrasonic wave propagation in dry and brine-saturated sandstones as a function of effective stress: laboratory measurements and modelling, *Geophys. prospect.,* **42,** 299–328.

Toksöz, M.N., Johnston, D.H. & Timur, A., 1979. Attenuation of seismic waves in dry and saturated rocks: I Laboratory measurements, *Geophysics,* **44,** 681–690.

Toksöz, M.N. & Johnston, D.H., (Eds), 1981. *Seismic Wave Attenuation*, Society of Exploration Geophysics, Tusla, Oklahoma.

Vernik, L., 1996. Predicting porosity from acoustic velocities in siliciclastics: a new look, *Geophysics,* **62,** 118–128.

Winkler, K.W. & Nur, A., 1979. Pore fluids and seismic attenuation in rocks, *Geophys. Res. lett.,* **6,** 1–4.

Winkler, K.W., 1985. Dispersion analysis of velocity and attenuation in Berea Sandstone, *J. geophys. Res.,* **90,** 6793–6800.

Winkler, K.W., 1986. Estimates of velocity dispersion between seismic and ultrasonic frequencies, *Geophysics,* **51,** 183–189.

Wulff, A.M., 1995. Absorptionsmechanismen bei Ultraschallwellen in fluidhaltigen Sandsteinen unter verschiedenen Druckbedingungen, *PhD thesis*, Technical University of Berlin, Berlin.

Wulff, A.M., 1996. Personal communication and Fortran routine.

Wulff, A.M. & Burkhardt, H., 1996. The Influence of local fluid flow and the microstructure on elastic and anelastic Rock Properties, *Surv. Geophys.,* **17,** 347–360.

Wulff, A.M. & Burkhardt, H., 1997. Mechanisms affecting ultrasonic wave propagation in fluid-containing sandstones under high hydrostatic pressure, *J. geophys. Res.,* **102,** 3043–3050.

Zimmerman, R.W., Somerton, W.H. & King, M.S., 1986. Compressibility of Rocks, *J. geophys. Res.,* **91,** 12 765–12 777.

Zimmerman, R.W., 1991. *Compressibility of Sandstones*, Elsevier, Amsterdam; Oxford; New York; Tokyo.

APPENDIX A: EQUATIONS OF THE NEW COMBINED MODEL

Shear wave

Replacing the real shear modulus N in the basic equations of Biot (1956) by the complex shear modulus N_{LF}, calculated with the formulas of Murphy *et al.* (1986) leads to the following equations describing the S wave:

$$\nabla^2\vec{\omega} = \frac{1}{N_{LF}}\frac{\partial^2}{\partial t^2}(\rho_{11}\vec{\omega} + \rho_{12}\vec{\Omega}) + b\frac{\partial}{\partial t}(\vec{\omega} - \vec{\Omega})$$

$$0 = \frac{\partial^2}{\partial t^2}(\rho_{12}\vec{\omega} + \rho_{22}\vec{\Omega}) - b\frac{\partial}{\partial t}(\vec{\omega} - \vec{\Omega}). \tag{A1}$$

The coupling parameters b, ρ_{12}, ρ_{11}, ρ_{22} are defined as:

$$\begin{aligned} b &= \frac{\eta\phi^2}{\kappa} \\ \rho_{12} &= (1-\alpha')\phi\rho, \\ \rho_{11} &= (1-\phi)\rho_s - \rho_{12}, \\ \rho_{22} &= \phi\rho - \rho_{12} \end{aligned} \tag{A2}$$

The coupling is influenced by the hydraulic permeability κ and the porosity ϕ of the rock and the dynamic viscosity η of the fluid as well as the density ρ of the gas–fluid mixture. After Berryman (1980) the dimensionless factor α' can lie be between 1 and 3.

For a plane wave with the frequency f and the complex wave number $l = l_r + il_i$

$$\begin{aligned} \vec{\omega} &= \vec{C}_1 \exp[i(lx + 2\pi ft)] = \text{rot}\,\vec{u} \\ \vec{\Omega} &= \vec{C}_2 \exp[i(lx + 2\pi ft)] = \text{rot}\,\vec{U} \end{aligned} \tag{A3}$$

is describing the mean displacement of the solid ($\vec{u} = (u_x,\ u_y,\ u_z)^T$) and fluid ($\vec{U} = U_x,\ U_y,\ U_z)^T$), respectively. Inserting A3 into equation A1 and eliminating the constants C_1 and C_2 the following relationship is obtained:

$$\frac{(l_r + il_i)^2}{(2\pi f)^2} = \frac{(E_r - iE_i)\rho}{N_{LF}} \tag{A4}$$

with

$$\begin{aligned} E_r &= \frac{1 + \gamma_{22}\frac{\gamma_{11}\gamma_{22} - \gamma_{12}^2}{(\gamma_{12}+\gamma_{22})^2}\left(\frac{f}{f_c}\right)^2}{1 + \left(\frac{\gamma_{22}}{\gamma_{12}+\gamma_{22}}\right)^2\left(\frac{f}{f_c}\right)^2} \\ E_i &= \frac{(\gamma_{22} + \gamma_{12})\left(\frac{f}{f_c}\right)}{1 + \left(\frac{\gamma_{22}}{\gamma_{12}+\gamma_{22}}\right)^2\left(\frac{f}{f_c}\right)^2} \\ \frac{f}{f_c} &= \frac{2\pi f\rho(\gamma_{12} + \gamma_{22})}{b} \\ \gamma_{11} &= \rho_{11}/\rho\,, \quad \gamma_{12} = \rho_{12}/\rho\,, \quad \gamma_{22} = \rho_{22}/\rho \\ \rho &= \rho_{11} + 2\rho_{12} + \rho_{22}. \end{aligned}$$

Eq. (A4) can be rewritten in the following way:

$$\frac{(l_r + il_i)^2}{(2\pi f)^2} = (\tilde{E}_r - i\tilde{E}_i) = \frac{\rho}{N_{LGF}} \tag{A5}$$

using

$$\begin{aligned} \tilde{E}_r &= \Re\left(\frac{(E_r - iE_i)\rho}{N_{LF}}\right) \\ \tilde{E}_i &= -\Im\left(\frac{(E_r - iE_i)\rho}{N_{LF}}\right). \end{aligned}$$

The comparison of the real and the imaginary part of eq. (A5) is leading to the phase velocity v_s and the attenuation $\frac{1}{Q_s}$:

$$\begin{aligned} v_s &= \frac{2\pi f}{l_r} = \sqrt{\frac{2}{\tilde{E}_b}} \\ \frac{1}{Q_s} &= -2\frac{l_i}{l_r} = -2\frac{\tilde{E}_i}{\tilde{E}_b} \end{aligned} \tag{A6}$$

with

$$\begin{aligned} l_r &= 2\pi f\sqrt{\tfrac{\tilde{E}_b}{2}} \\ l_i &= 2\pi f\frac{\tilde{E}_i}{\sqrt{2\tilde{E}_b}} \\ \tilde{E}_b &= \tilde{E}_r + \sqrt{(\tilde{E}_r)^2 + (\tilde{E}_i)^2}. \end{aligned}$$

A2 Compressional wave

The basic equations for the P wave after Biot (1956a) are:

$$\begin{aligned} \nabla^2[Pe + Q\epsilon] &= \frac{\partial^2}{\partial t^2}(\rho_{11}e + \rho_{12}\epsilon) + b\frac{\partial}{\partial t}(e - \epsilon) \\ \nabla^2[Qe + R\epsilon] &= \frac{\partial^2}{\partial t^2}(\rho_{12}e + \rho_{22}\epsilon) - b\frac{\partial}{\partial t}(e - \epsilon) \end{aligned} \tag{A7}$$

with P, Q, R being elastic constants. The coupling parameters b, ρ_{12}, ρ_{11}, ρ_{22} are given in eq. (A2). Defining the complex wave number $k = k_r + ik_i$ and inserting

$$\begin{aligned} e &= C_1 \exp[i(kx + 2\pi ft)] = \text{div}\vec{u} \\ \epsilon &= C_2 \exp[i(kx + 2\pi ft)] = \text{div}\,\vec{U} \end{aligned} \tag{A8}$$

into eq. (A7), setting $b = 0$ and eliminating the constants C_1 and C_2 is leading to the following equation for the determination of $y = k^2/(2\,\pi\,f)^2$:

$$b_1 y^2 - b_2 y + b_3 = 0 \tag{A9}$$

with

$$b_1 = (PR - Q^2)$$

$$b_2 = (P\rho_{22} + R\rho_{11} - 2Q\rho_{12})$$

$$b_3 = \left(\rho_{11}\rho_{22} - \rho_{12}^2\right).$$

The solution of eq. (A9) (fluid motion is not attenuated, $b = 0$) is leading to the square of the reciprocal complex velocities $\frac{1}{v_{p'1/2}^2}$ of the P wave:

$$y_1 = \frac{1}{v_{p'1}^2} = \frac{b_2 - h_2}{2b_1}$$

$$y_2 = \frac{1}{v_{p'2}^2} = \frac{b_2 + h_2}{2b_1} \tag{A10}$$

with

$$h_2 = \sqrt{b_2^2 - 4b_1 b_3}$$
$$= \sqrt{(P\rho_{22} + R\rho_{11} - 2Q\rho_{12})^2 - 4(PR - Q^2)\left(\rho_{11}\rho_{22} - \rho_{12}^2\right)}.$$

After Biot & Willis (1957) the constants Q, R, P and H are defined as:

$$Q = \frac{(1 - \phi - \frac{K_b}{K_s})\phi K_s}{1 - \phi - \frac{K_b}{K_s} + \phi\frac{K_s}{K_f}}$$

$$R = \frac{\phi^2 K_s}{1 - \phi - \frac{K_b}{K_s} + \phi\frac{K_s}{K_f}}$$

$$P = \frac{(1-\phi)(1 - \phi - \frac{K_b}{K_s})K_s + \phi\frac{K_s}{K_f}K_b}{1 - \phi - \frac{K_b}{K_s} + \phi\frac{K_s}{K_f}} + \frac{4}{3}N\,. \tag{A11}$$

Again the real moduli K_b and N of the rock matrix have to be replaced by the complex moduli K_{LF} and N_{LF} calculated using the formulas of Murphy *et al.* (1986). Using the solutions $y_{1/2}$ the basic eq. (A7) with $b \neq 0$ (i.e. viscosity $\eta \neq 0$) can be reformulated by using a harmonic formulation and elimination of the constants C_1 and C_2:

$$0 = b_1 y^2 - b_2 y + b_3 + \frac{ib}{2\pi f\rho}(y - 1)$$
$$= y^2 - \left[(y_1 + y_2) - iM\frac{\rho}{H}\right]y + y_1 y_2 - i\frac{\rho^2}{H^2}$$
$$= \frac{k^4}{(2\pi f)^4} - \left[\frac{1}{v_{p'1}^2} + \frac{1}{v_{p'2}^2} - iM\frac{\rho}{H}\right]\frac{k^2}{(2\pi f)^2}$$
$$+\frac{1}{v_{p'1}^2}\frac{1}{v_{p'2}^2} - iM\frac{\rho^2}{H^2}, \tag{A12}$$

with

$$M = \frac{\rho_{12} + \rho_{22}}{(PR - Q^2)}\frac{H^2}{\rho}\frac{f_c}{f}$$

and

$$H = P + R + 2Q \Rightarrow H = \frac{\left(1 - \frac{K_b}{K_s}\right)\phi K_s}{1 - \phi - \frac{K_b}{K_s} + \phi\frac{K_s}{K_f}} + K_b + \frac{4}{3}N.$$

The solution of eq. (A12) reveals:

$$\sqrt{y_3} = \frac{(k_r + ik_i)}{(2\pi f)}_1 = \sqrt{(h_1 - \sqrt{h_3})} = \sqrt{\frac{\rho}{M}}_1$$
$$\sqrt{y_4} = \frac{(k_r + ik_i)}{(2\pi f)}_2 = \sqrt{(h_1 + \sqrt{h_3})} = \sqrt{\frac{\rho}{M}}_2 \tag{A13}$$

with

$$h_1 = \frac{1}{2}\left[\frac{1}{v_{p'1}^2} + \frac{1}{v_{p'2}^2} - iM\frac{\rho}{H}\right] h_3 = (h_1)^2 - \frac{1}{v_{p'1}^2}\frac{1}{v_{p'2}^2} + iM\frac{\rho^2}{H^2}$$

The velocities and attenuations of the global–local fluid flow model can be calculated using the values $\sqrt{y_3}$ and $\sqrt{y_4}$, respectively:

$$v_{p1} = \frac{2\pi f}{k_r}_1 = \frac{1}{\Re(\sqrt{y_3})} \quad v_{p2} = \frac{2\pi f}{k_r}_2 = \frac{1}{\Re(\sqrt{y_4})}$$
$$\frac{1}{Q_{p1}} \approx 2\frac{k_i}{k_r}_1 = 2\frac{\Im(\sqrt{y_3})}{\Re(\sqrt{y_3})} \quad \frac{1}{Q_{p2}} \approx 2\frac{k_i}{k_r}_2 = 2\frac{\Im(\sqrt{y_4})}{\Re(\sqrt{y_4})}. \tag{A14}$$